

Cooperative dynamics in auditory brain response

J. Kwapien¹, S. Drożdż^{1;2}, L. C. Liu³ and A. A. Ioannides^{3;4;5}

¹ Institute of Nuclear Physics, PL-31-342 Kraków, Poland,

² Institut für Kernphysik, Forschungszentrum Jülich, D-52425 Jülich, Germany,

³ Institut für Medizin, Forschungszentrum Jülich, D-52425 Jülich, Germany,

⁴ Physics Department, The Open University, Milton Keynes, MK7 6AA, UK,

⁵ Laboratory for Human Brain Dynamics, BSI, The RIKEN Institute, Hirosawa 2-1, Wako-shi

351-01, Japan

(October 27, 2021)

Abstract

Simultaneous estimates of the activity in the left and right auditory cortex of five normal human subjects were extracted from multichannel magnetoencephalography recordings. Left, right and binaural stimulation were used, in separate runs, for each subject. The resulting time-series of left and right auditory cortex activity were analysed using the concept of mutual information. The analysis constitutes an objective method to address the nature of inter-hemispheric correlations in response to auditory stimulations. The results provide a clear evidence for the occurrence of such correlations mediated by a direct information transport, with clear laterality effects: as a rule, the contralateral hemisphere leads by 10–20 ms, as can be seen in the average signal. The strength of the inter-hemispheric coupling, which cannot be extracted from the average data, is found to be highly variable from subject to subject, but remarkably stable for each subject.

PACS numbers: 05.60.+w, 43.64.-q, 84.35.+i, 87.40.+w

I. INTRODUCTION

Two emergent properties of complex systems are collectivity and chaos. Both properties are relevant for biological systems which some believe are balanced at the interface of collectivity and chaos [1]. The brain itself has been described in these terms, particularly its tendency to diversity and its ability of generating coherent patterns of activity, switching continuously from one to another. These properties are also expected to be very useful for describing how local cortical specialization is efficiently co-ordinated by functional global integration mechanisms [2]. Implicit in any such explanatory description is the brain's activity on various space and time scales.

A quantitative understanding of the hierarchy of the underlying structures, both in space and in time, is of fundamental importance for a proper design of a unified theoretical model (for some attempts in this direction see for instance ref. [3]) relating local neuronal dynamics and global attributes of sensory processing. This, however, is an extremely difficult problem since the conscious human brain is never at rest; central control of body function and regulation, seeing thoughts and feelings, ensure that even in the most relaxed state a tapestry of regional activations is woven every instant. Even the simplest of acts engages a multitude of areas in a way that varies even as the same task is repeated many times. We have studied one of the simplest possible brain responses: the activity in the human auditory cortex, elicited by the presentation of simple tones, delivered regularly to one or both ears. Even in this very simple and artificial scenario animal [4] and human studies [5,6] have shown that many different areas are involved. Nevertheless, for this case the two auditory areas are known to be active and prominent. Magnetoencephalography (MEG) [7] is particularly appropriate in the present context, because activity from the auditory cortex is readily identifiable from both the average MEG signal [8,9] and in single trials [10,11]

Furthermore, since the two auditory cortices are well separated on either side of the head, the instrument at our disposal, with two separate probes each with 37 channels, was ideal for mapping the magnetic signal: while one probe is sensing the signal over the left auditory cortex the other is sensing the signal over the right auditory cortex. With optimal sensor location, a very simple linear combinations of signals can be established to map the activity in each auditory cortex. In effect we make from each 37 channel sensor array a Virtual Sensor (VS) which registers the activity in the adjacent auditory cortex [11].

MEG is a completely non-invasive method of measuring the distribution and time dependence of the magnetic field outside the skull. Just like the more conventional Electroencephalography (EEG) it allows to time-resolve neuronal activity on the scale of 1ms [12]. Its main advantage over scalp-EEG is that the skull and the scalp are transparent to the magnetic field and, therefore, an external measured magnetic field is not distorted by radial conductivity effects. Furthermore, magnetic fields outside the skull are generated predominantly by the currents tangential to the surface of the head. The cortical currents are perpendicular to the surface of the cortex but almost 70% of the human cortex is folded into sulci which makes these currents effectively tangential to the skull and, thus, accessible to MEG. The above aspects of MEG make it particularly suitable for studying the spatio-temporal characteristics of the brain dynamics (e.g. [13]). The details of the MEG experiments used to generate the data analysed in this paper are presented in Section 2.

In MEG the response to a stimulus is represented by the time-series, one time-series for

each channel. We use the repetition of identical stimulus presentations (commonly refer to as trials or epochs) to compute statistical measures of correlations or of complexity. We use the mutual information (MI) [14], a concept related to entropy, to characterise the correlation between the two time-series representing the left and right auditory cortex activity in a single trial. An outline of the corresponding formalism, including a very useful generalization of MI, is given in Section 3. This formalism is then used in Section 4 to study the long-range cortical correlations induced by left-ear, right-ear and binaural auditory stimulations. The paper ends with some concluding remarks.

II. DESCRIPTION OF EXPERIMENT

The measurement of the minute magnetic field generated by the coherent activity of many millions of neurons can be recorded almost routinely today, using super Quantum Interference Devices (SQUIDs) operating within shielded environment [7]. The most advanced instruments today have well over 100 SQUIDs allowing for a fairly dense coverage of sensors all round the head. In this work we will report a study performed with the twin MAGNES system of Biomagnetic Technologies inc. (BTi) in San Diego. This system has two separate dewars each with 37 first order gradiometers. During the experiment, the subject's head was resting on the bottom dewar, while the top dewar was placed over the opposite temporal area. Five healthy male volunteers (age: 37.8 \pm 9.7) gave their informed consent to participate in two experiments. Four subjects (JD, JL, FB and RB) were right handed, two of them (FB and RB) were twins and one subject (DB) was left handed. The first experiment, was in two parts (Ex1a and Ex1b), with a second experiment, Ex2, performed between Ex1a and Ex1b. The second experiment used similar auditory tones in a standard GO/NOGO symmetric avoidance protocol. For the purpose of this study the details of Ex2 are not relevant, other than it was long and it involved auditory stimuli which determined whether or not a movement was to be made or withheld. For more details see [11]. The subject maintained the same position throughout Ex1 and Ex2, which was fixed as follows: A standard auditory evoked response was first obtained from stimuli delivered to both ears. This response is termed M100, it is the magnetic analogue of the N100, a peak in the EEG signal corresponding to the crest of a negative potential [12]. The BTi software was used to compute and display the average signal across 120 single trials, while the subject remained in place. The inspection of the average signal was used to guide repositioning of the dewars so that the prominent M100 peak was captured with the positive and negative fields evenly covered by the sensors in each probe. The procedure was repeated until each dewar was well positioned, usually in one to three placements. Two further runs were obtained with this optimal dewar position with exactly the same protocol, but with the stimulus delivered first to the left and then to the right ear. The first part of Ex1 (Ex1a) consisted of three runs: the last dewar placement run with binaural stimuli and the two monaural stimulations. The subject then underwent the more demanding and long Ex2. Immediately after Ex2, with the subject still holding the same position, experiment Ex1 was repeated (for most subjects the binaural tone presentation was omitted). For both the positioning runs and the 5 or 6 actual runs of Ex1, the stimuli were 50 msec, 1 kHz tone bursts at 50dB (10 msec rise/fall and 30 msec plateau). The inter-stimulus interval was 1 second (\pm 20 msec). The MEG signal was recorded in continuous mode, sampled at 1042 Hz and filtered in real time with

0.1 Hz high pass. The analysis to be reported in this paper used two more signals obtained by further band-pass filtering in the 1-200 Hz (with notch filters at 50 Hz, 100 Hz and 150 Hz), and 3-20 Hz.

The biomagnetic inverse problem has no unique solution. This seemingly unsurmountable obstacle becomes less formidable when physiological constraints are introduced and provided the resolution demanded from the data is limited to what is achievable given the sparseness of the sensors and the noise in the data. The extraction of reliable estimates is considerably easier for superficial generators, directly below a sensor array, i.e. the auditory cortex in our case. The requirement to analyze single trials poses new problems. We have arrived at a simple but very efficient solution beginning with powerful, but computationally demanding methods, and an analytic transformation of the signal, the V_3 [10]. Comprehensive tests with computer generated data have shown that a virtual sensor (VS), can be designed to respond preferentially to activations of superficial focal source. This is similar to earlier work using a template approach [10], but here it has been specially developed in the context of the 37 channel MAGNES system to obtain regions of interest rapidly. For the purposes of our investigation a good VS for auditory cortex activation can be easily obtained from each probe, provided the 37 channels on each side capture symmetrically the dipolar field distribution at the peak of the average signal. For each probe, we have identified the two channels (k_1 and k_2), which produced the maximum difference at the time of the M100 peak, and used them to define the composite VS,

$$V S^{M 100}(t) = \sum_{j=1}^{37} \frac{r_j^2}{4} e^{-\frac{r_j - r_{k_1 j}}{2}} e^{-\frac{r_j - r_{k_2 j}}{2}} S_j(t) \quad (1)$$

where λ is the characteristic length (we have used $\lambda = 0.02$ m which is roughly the inter-channel separation); the results do not depend critically on this value. $S_j(t)$ is the MEG signal at time t recorded by the j^{th} channel, whose position vector is r_j .

The coefficients of the expansion are computed at the time of the M100 peak in the average signal; these coefficients are used unchanged for the analysis of all single trials. The computation of VS is very fast and hence VS can be used to scan through all MEG averaged or single trial signals very quickly. For the purpose of this present study the VS output from each probe provides a good estimate of the activity in each auditory cortex. We can therefore use the pair of time-series in each single trial to study the relationship between the left and right cortex activity.

Fig. 1 summarizes the setup (a), shows a typical set of MEG signals (b) and highlights the area of strong sensitivity for the VS corresponding to this signal.

III. MUTUAL INFORMATION AND ITS GENERALIZED VERSION

In an experiment as described above the message about the subsystem s (brain area in this case) behavior is transmitted across the channel of instruments and procedures, and as a result, is represented by the time-series $x_s(t_n)$. The subscript n indicates that experiment determines x_s at the discrete time points and thus induces a partition of the phase space of s . This time-series maps out the probability $p(j)$ that $x_s(t_n)$ assumes value characteristic

for the j th element of the partition. The average amount of information gained from such a measurement can be quantified in terms of the entropy

$$H(X_s) = - \sum_j p(j) \ln p(j); \quad (2)$$

where X_s denotes the whole set of possible messages and the associated probabilities ($\sum_j p(j) = 1$) for the subsystem s .

If two subsystems, s_1 and s_2 are measured simultaneously, as is the case here, then the corresponding probability distributions are $p(j_1)$ and $p(j_2)$, and the most relevant one, the joint distribution $p(j_1; j_2)$. For the combined system, composed of s_1 and s_2 , the joint entropy $H(X_{s_1}; X_{s_2})$ has the form analogous to eq. 2. It is easy to verify that

$$H(X_{s_1}; X_{s_2}) = H(X_{s_1}) + H(X_{s_2}) \quad (3)$$

and the equality holds only if s_1 and s_2 are statistically independent, i.e., $p(j_1; j_2) = p(j_1)p(j_2)$. The quantity

$$I(X_{s_1}; X_{s_2}) = H(X_{s_1}) + H(X_{s_2}) - H(X_{s_1}; X_{s_2}) \quad (4)$$

thus evaluates the amount of information about one of the subsystems resulting from a measurement of the other and is therefore called the mutual information. Generalization of this concept to a larger number of subsystems is straightforward and is known as redundancy [15].

A question of fundamental interest, especially in the context described in the Introduction, is whether the spatiotemporal correlations between the subsystems are caused by spatial uniformity or by information transport. Information transport may lead to time-delayed effects in the synchronization of correlations. Such effects can easily be quantified by calculating the time-delayed mutual information between measurements of the two subsystems at different times. The corresponding prescription retains of course the structure of Eq. 4; only the time-series $x_{s_1}(t)$ needs to be correlated with $x_{s_2}(t + \tau)$. The mutual information $I(X_{s_1}; X_{s_2}; \tau)$ then becomes a function of the time-delay τ . It may display maximum at a certain finite value of τ . This value of τ thus provides an estimate on the time needed for the information to be transported from the subsystem s_1 to s_2 .

There exists [16] an interesting generalization of the concept of the information entropy. It reads:

$$H_q(X_s) = \frac{1}{1-q} \ln \sum_j p^q(j) \quad (5)$$

For $q \rightarrow 1$ this equation yields the standard information entropy [Eq. 2]. The most useful property of $H_q(X_s)$ is that with increasing q a higher weight is given to the largest components in the set $\{p(j)\}$. This proves very instructive in studying various aspects of the phase-space exploration in dynamical systems [17]. Since normally the largest components are likely to dominate the process of correlating the two subsystems it seems worthwhile to introduce analogous generalization at the level of mutual information. In fact, recent literature [18] considers such a generalization but mostly for $q = 2$ and on a formal level, without fully documenting its utility in practical terms.

By making use of the defining equation 4, $H_q(X_s)$ of Eq. 5, the corresponding generalized joint entropy and allowing the time-delay between the time-series, after simple algebra one obtains the following expression for the generalized mutual information:

$$I_q(X_{s1}; X_{s2}; \tau) = \frac{1}{1-q} \ln \frac{\sum_{j_1, j_2} p^q(j_1) p^q(j_2)}{\sum_{j_1, j_2} p^q(j_1; j_2; \tau)} \quad (6)$$

This equation constitutes a basis for numerical applications and its utility will be illustrated in the next Section.

A reliable estimate of the entropy requires appropriately accurate sampling rate in order to realistically determine the probability distribution $p(j)$. For this one needs either a sufficiently long single time-series representing a phenomenon of interest or, as in the present case of the relatively short time-series, one needs a sufficiently large ensemble of such series. When estimating I_q in the latter case one thus faces the two possibilities: (i) I_q is calculated independently from each time-series and then averaged over an ensemble or (ii) the ensemble averaged probability distribution is used in Eq. 6. Obviously, in general the two operations are not equivalent for this simple reason that the logarithm and the sum do not commute. It is quite natural to expect that the prescription (ii) is more appropriate as it results in a smoother behavior already on the level of probability distributions, and thus the final result is to a lesser degree contaminated by artificial noisy fluctuations. This statement can be confirmed by explicit numerical verification.

From a general point of view one note of caution is also needed at this point regarding I_q . For $q > 1$ it may happen that it assumes small negative values and the fact that it reaches a zero value does not automatically mean that the subsystems are statistically independent. An inverse implication still holds, however, as for $q = 1$: Subsystems which are statistically independent lead to $I_q = 0$. Also, the positive value of I_q for any q means that the subsystems are not independent. What in this connection is important for us is that the above peculiarity of I_q for $q > 1$ may apply to the region of very weak correlations only.

IV. RESULTS

Little can be extracted from a single pair of time-series. We need to consider the ensemble of single trials. We first establish the notation.

From here on we will restrict our attention to the VS output computed as described in Section 2. Each run is represented by two sets of the time series covering the 1s long time-interval $x_L(t_n)$ and $x_R(t_n)$ ($n = 1; \dots; 1042$, corresponding to the left (L) and the right (R) hemisphere, respectively). The sampling rate is 1042 Hz, so $t_{n+1} - t_n = 0.96\text{ms}$). The superscript $= 1; \dots; 120$ labels the single trials in each experiment. The time-series are consistently centered such that the onset of the stimulus corresponds to $n = 230$. Fig. 2 shows three typical, randomly selected, single-trial raw time-series together with the average

$$x_{L,R}(t_n) = \frac{1}{N} \sum_{i=1}^N x_{L,R}^i(t_n) \quad (7)$$

over all $N = 120$ trials for the left (a) and right (b) hemisphere signals, for one subject (JD).

It is difficult to identify the stimulus onset from the raw single-trial signal, although a relationship between the peak of the average response can be seen in some of the single trials. For a more detailed discussion about the relationship between the average signal and the average see [10,11]. It is clear that the single trial activity is not dominated by the stimulus. Since the background brain activity is not time-locked to the stimulus it is averaged out after summing up a sufficiently large number of identical trials. The average over the full set of our 120 consecutive trials exhibits a pronounced M 100 peak centered at around 100ms after the stimulus onset. At the time of the M 100 a number of generators are active; our sensor positioning and the VS analysis in each hemisphere disentangles from the MEG data the local collective neuronal response at the superficial part of the auditory cortex. Interestingly, even though the stimulus is applied asymmetrically (left ear) a similar (but not identical) structure is detected on both hemispheres. This is consistent with the known auditory pathways which are less segregated on the contralateral side than in other sensory modalities, namely the visual and somatosensory; an additional contribution may arise from long-range interaction between the two cortical auditory areas, which are also known to be heavily interconnected via the corpus callosum.

We first explore the variation of mutual information between the two hemispheres both, as a function of the time-delay and as a function of the frequency. The frequency spectrum of the input data series $x_{L,R}(t_n)$ is determined by their discrete Fourier transform as

$$X_{L,R}(k) = \sum_{n=1}^N x_{L,R}(t_n) \exp(2\pi i k n / N); \quad (8)$$

$X_{L,R}(k)$ being the complex numbers ($X_{L,R}(k) = \Re_{L,R}(k) + i \Im_{L,R}(k)$). By inverting this transformation in a reduced interval $k \in [K, K+2\pi]$ of discrete frequencies k one obtains the filtered series $x_{L,R}^{K;K}(t_n)$ spanning the frequency window K centered at K :

$$x_{L,R}^{K;K}(t_n) = \frac{1}{K} \sum_{k=K}^{K+2\pi} X_{L,R}(k) \exp(2\pi i k n / N); \quad (9)$$

Determining a minimum value of K which can safely be used in the present context requires some care. The point is that its too small value may generate artificial correlations in the mutual information of filtered time-series. In an extreme limit, one frequency component will always be correlated in some way. What preserves or washes out the correlations in finite frequency windows is the relation among amplitudes of different frequency components. We determine a reasonable minimum value of K , such that no artificial correlations are induced, self-consistently: we make use of the surrogate time-series of the original ones. The surrogates are obtained by randomizing the phases $\phi(k)$ of $X_{L,R}(k)$ and making use of Eq. 9. This operation preserves the power spectrum of the original series. By calculating the mutual information of the so generated surrogates of $x_L(t_n)$ and $x_R(t_n)$ we find K equivalent to 4 Hz as an appropriate minimum frequency window for our data. Below this value some correlations may show up even on the level of surrogates.

Fig. 3 shows the landscape of the mutual information ($q = 1$) in the time-delay and in the frequency window of 5 Hz centered at the value indicated. This is one of the experiments on subject JD. The results of the other experiments for the same subject look similar.

When making use of Eq. 6, here, as well as in the whole following discussion, a grid of 10 bins covering an interval of variation of both, $x_R(t_n)$ and $x_L(t_n + \Delta t)$ is introduced. This guarantees stability of the results. For a given experiment the three different probability distributions entering Eq. 6 are evaluated by superimposing histograms corresponding to all the time-series ($n = 1; \dots; 120$) and then the logarithm is taken. As mentioned before, one could also calculate MI for each n separately and then average over n but for the present data such a procedure turns out highly unsatisfactory in terms of statistics; it results in a much higher level of noisy background fluctuations.

The MI displayed in Fig. 3 is calculated from the whole 1s ($n = 1; \dots; 1042$) time-interval. Its specific dependence will be discussed in full detail later and Fig. 3 is basically supposed to illustrate the frequency localization of significant correlations. As it is clearly seen, such correlations are mediated by the low-frequency (up to 20 Hz) activity. This picture turns out to be subject independent. The amplitude of MI is found to depend from subject to subject, however. For certain subjects the correlations are so weak that they are hardly identifiable on the level of $q = 1$ MI. For this reason we first explore a possible advantage of using the generalized MI as allowed by Eq. 6. According to the above frequency localization, and in order to make the following study more transparent, all the time-series used will be filtered to the frequency window between 3 and 20 Hz. Furthermore, since correlations are mainly connected with appearance of the M100 peak, the time-series will be truncated to the interval between $i = 230$ and $i = 491$. This covers 250ms starting exactly at the initial moment of the stimulus.

The benefit of using the higher q -MI is documented in Fig. 4. This figure illustrates the q -dependence ($q = 1; 2; 4; 6$) of the generalized mutual information for the two examples: of strong correlations (JD) and of weak correlations (FB). Clearly, the higher q -values offer a much more precise estimate of the time-delay at maximum. This originates from the fact that increasing q gives a higher weight to larger components in the probability distribution and this turns out especially important for the cases of weak correlations. For this reason a summary of the results of all experiments, for all live subjects, as displayed in Fig. 5, is done for $q = 6$. A convention used in the corresponding calculation when defining the sign of the time-delay between $x_L(t_n)$ and $x_R(t_n + \Delta t)$ is such that its negative value means that a relevant excitation in the right hemisphere is time-advanced relative to the left hemisphere. Of course, the opposite applies for positive sign.

Several conclusions are to be drawn from Fig. 5a. First of all, the correlations under study are spatially nonuniform and the information transport between the hemispheres takes about 10ms. The relative location of the peaks in MI indicates that, at least statistically, the contralateral hemisphere drives the response for all the subjects and conditions studied. This, however, in general can only be identified by a parallel analysis of the left versus right ear stimulation (binaural is also helpful) of the same subject. The point is that for some subjects there are certain asymmetry effects. For instance, in JL the ipsilateral hemisphere somewhat overtakes (~ 5 ms) when the right ear is stimulated but then the contralateral hemisphere overtakes even more when the tone is delivered to the other ear, so that the relative location of the peaks in MI, corresponding to the left and right ear stimulation, respectively, is still preserved. This asymmetry in JL disappears in the experiment Ex1b, however. A trace of asymmetry, but in opposite direction, is also visible in JD; again more in Ex1a than in Ex1b. A likely explanation of those asymmetry effects is that we are facing

a superposition of the two phenomena. One is a leading role of the contralateral hemisphere when the tone is delivered to one ear (either left or right) and the other may originate from certain subject specific asymmetry in properties of the left and right auditory areas. The latter kind of asymmetry is known to occur quite frequently [12].

Figs. 5b and 5c illustrate the same quantities for the time-intervals just before the stimulus onset (-230 ± 0 ms) and soon after the M100 period (251 ± 500 ms), respectively. The picture changes significantly. Except for JD the correlations essentially disappear. JD seems to display certain permanent inter-hemispheric correlations but here they are considerably weaker and always driven by the left hemisphere. This supports the claim that the correlations under study are primarily associated with the stimulus.

Another interesting quantity is the strength of information transfer between the hemispheres. This characteristic measured in terms of the MI-excess over background is largely invariant for a given subject (similar for different experiments). It is, however, strongly subject dependent and ranges between very pronounced (JD) and rather weak (FB, RB). A related question that emerges in this connection is whether this effect results from different strength of the coupling between the hemispheres or, whether this is due to the fact the local M100 excitations differ in their degree of collectivity. That the second possibility is more likely to apply here can be concluded from Fig. 6 which shows the averaged (over 120 trials) MEG time-series for JD, DB, JL and FB (RB looks similar to FB). This figure illustrates both, the left and the right hemisphere responses generated by the left, right and binaural stimulations. The results shown also display left/right hemispheric asymmetry for JD and JL, oriented consistently with the results of Fig. 5a. The magnitude of amplitude of the so quantified response reflects a degree of neuronal synchrony developing the M100 complex in each case and this amplitude goes in parallel with the strength of the information transport (Fig. 5a). This, in a sense, is natural since the amount of information to be communicated results from the original local collectivity. It is also consistent with the low-frequency origin of inter-hemispheric correlations as illustrated in Fig. 3. Localization in frequency means higher synchrony and more determinism, and these, in general, constitute preferential conditions for the long-range inter-hemispheric correlations to occur.

Such conclusion gets further support from the structure of the power spectrum (squared modulus of the Fourier transform) of the time-series. These power spectra are calculated from the original time-series $x_{L,R}(t)$ representing the whole specific experiment lasting 120s and are shown in Fig. 7 for the two extreme cases, JD and FB, respectively. The cases of stronger correlations (JD) are accompanied by the power spectra that have the lower-frequency part significantly amplified relative to the cases of weak correlations (FB, RB). The opposite applies to the high-frequency region. The weak correlations are thus connected with a more noisy dynamics which acts destructively on local coherence and, consequently, on long-range correlations. It is however interesting to notice that even in this case the power spectrum is not completely flat as for the white noise phenomena but shows a nice " $1=f$ "-type (straight line of finite negative slope in the log-log scale) behavior [19]. For JD this behavior is not that nice but the deviation seems to be largely attributable to the permanent activity at 8 Hz (α -rhythm), consistent with the previous discussion. In fact, this kind of power-spectrum one may anticipate already by looking at the M100 waveform seen in the average signal (Fig. 6) and taking into account its functional similarity to the QRS complex of the electrocardiogram. This complex develops the inverse power-law spectrum

which some interpret in terms of the fractal character of the cardiac His-Purkinje conduction system [20]. In the present context this perhaps signals that the evolution of the M 100 may be governed by a phenomenon of self-organized criticality [21] which is a more catastrophic form of collectivity and is generated by a fractal (scale-invariant) 'avalanche'-like process. Interestingly, a new class of neural networks based on adaptive performance networks [22] shows exactly this type of power spectra. It also allows some local deviations from this behavior and those deviations result from certain subject specific stronger activity at some frequency. This model involving the elements of self-organized criticality can be trained [23] to react 'intelligently' to external sensory signals.

Of course, because of a strong permanent brain's activity, it is much more difficult to precisely disentangle from the background a contribution to the MEG power spectrum of a specific structure such as M 100. Therefore, the discussion related to Fig. 7 can only be treated as an indication that the M 100 complex may itself obey an inverse power-law. On the level of average time-series (Fig. 6) it can also be verified that it does although the statistics is then poorer. The related questions are, however, not the central issue of the present paper and will be the subject of our independent, more systematic, future study, both on the experimental as well as on the theoretical level.

Finally, on a way towards understanding the mechanism of inter-hemispheric correlations, it is instructive to look at MI between $x_L(t)$ and $x_R^+(t)$ for $\epsilon \neq 0$. Fig. 8 shows that, surprisingly, such correlations are much weaker for both subjects (as well as for all remaining). This result indicates that what actually correlates the opposite hemispheres in the present context is not just an independent appearance of M 100 in both hemispheres but the real inter-hemispheric information transport which projects one M 100 into another and thus induces certain similarity between them. They are thus functionally related and this is what the mutual information reflects. On the other hand the specific evolution of M 100 with respect to consecutive trials must involve nondeterministic elements which make the above, translated correlations much weaker. This means that only the global aspects of M 100 are time-locked to the stimulus; a detailed 'microscopic' evolution turns out largely stochastic. In fact, such a picture is again consistent with the phenomenon of self-organized criticality.

Besides the inter-hemispheric information transport discussed above there potentially exists another mechanism capable of introducing a time delay in the mutual information, namely a common driver which independently activates each path at separate times. Such a mechanism does not, however, seem to be able to explain such a significant change of correlations as shown in Fig. 8.

V. CONCLUSIONS

The present study provides a clear quantitative evidence for two levels of dynamical cooperation in the brain auditory processing. One is the local hemispheric collective response, reaching its maximum at about 100ms (M 100) after a stimulus onset. An interesting emerging aspect of this excitation is that its only global characteristics are time-locked to a stimulus. The underlying neuronal degrees of freedom involved are likely to significantly differ from trial to trial and a possible scenario potentially able to reconcile these two aspects is self-organized criticality. In fact, the structure of the corresponding power spectra is consistent with such a scenario. It also goes in parallel with our recent suggestion that

the single trial activity induced in the auditory cortex by a simple tone cannot be treated as a deterministic response emerging from a noisy background [10,11]. The second level of cooperation is the communication between the two hemispheres. The most conclusive in this connection are the monaural stimulations. The analysis then shows that, at least statistically, the contralateral hemisphere systematically leads by 10-20ms. The mechanism of this communication carries the signature of (delayed) synchronization and thus can be hypothesised as a direct information transport between the hemispheres.

An independent conclusion to be drawn from our study is that the mutual information (MI) and, especially, its generalization, provides a useful and statistically appropriate formalism for studying the temporal aspects of correlations in complex dynamical systems, even if, as here, such systems are represented by relatively short time-series.

This work was supported in part by Polish KBN Grant No. 2 P 03B 140 10.

REFERENCES

- [1] S.A. Kauffman, *The Origins of Order { Self-Organization and Selection in Evolution*, (Oxford University Press, Oxford, 1993)
- [2] K.J. Friston, G. Tononi, O. Sporns, and G.M. Edelman, *Hum. Brain Mapp.* 3, 302 (1995)
- [3] H. Sompolinsky, D. Golomb, and D. Kleinfeld, *Phys. Rev. A* 43, 6990 (1991);
D. Hansel and H. Sompolinsky, *Phys. Rev. Lett.* 68, 718 (1992);
M. Tsodyks, I. Mitkov, and H. Sompolinsky, *Phys. Rev. Lett.* 71, 1280 (1993);
J.J. Hopfield, *Nature* 376, 33 (1995);
U. Ernst, K. Pawelzik, and T. Geisel, *Phys. Rev. Lett.* 74, 1570 (1995);
W. Wang, G. Chen, and Z.D. Wang, *Phys. Rev. E* 56, 3728 (1997);
P.C. Bressler and S. Coombes, *Phys. Rev. Lett.* 78, 4665 (1997)
- [4] L. Aitkin, *The Auditory Cortex*, (Chapman and Hall, 1990)
- [5] W.R. Go, T. Allison, W. Lyons, T.C. Fisher, and R. Conte, *Progress in Clinical Neurophysiology*, vol. 2, ed. J.E. Desmedt, (Basel, Karger, 1977), p. 30-44
- [6] J.L. Lauter, P. Herscovitch, C. Formby, and M.E. Raichle, *Hear Res.* 20, 199 (1985)
- [7] M. Hamalainen, R. Hari, R.J. Ilmoniemi, J. Kuutila, and O. Lounasmaa, *Rev. Mod. Phys.* 65, 413 (1993)
- [8] R. Hari, *Advances of Audiology*, vol. 6, ed. F. Grandori, M. Hoke, and G.L. Romani, (Basel, Karger, 1990) p.222-282
- [9] K.D. Singh, A.A. Ioannides, N. Gray, H. Kober, H. Pongratz, A. Daun, P. Grummich, and J. Vith, *Electroenceph. clin. Neurophysiol.* 92, 365 (1994)
- [10] L.C. Liu and A.A. Ioannides, *Brain Topogr.* 8 (4), 385 (1996)
- [11] L.C. Liu, A.A. Ioannides and H.W. Muller-Gartner, *Electroenceph. clin. Neurophysiol.* 106, 64 (1998).
- [12] O.D. Creutzfeldt, *Cortex Cerebri*, (Oxford University Press, Oxford, 1995)
- [13] V.K. Jirsa, R. Friedrich, and H. Haken, *Physica D* 89, 100 (1995)
- [14] A.M. Fraser, and H.L. Swinney, *Phys. Rev. A* 33, 1134 (1986);
J.A. Vastino and H.L. Swinney, *Phys. Rev. Lett.* 60, 1773 (1988);
K. Matsumoto and I. Tsuda, *J. Phys. A* 21, 1405 (1988)
- [15] A.M. Fraser, *IEEE Trans. Inform. Theory* IT-35, 245 (1989)
- [16] A. Renyi, *Probability Theory* (North Holland, Amsterdam, 1970)
- [17] S. Drozd, S. Nishizaki, J. Wambach, and J. Speth, *Phys. Rev. Lett.* 74, 1075 (1995)
- [18] B. Pompe, *J. Stat. Phys.* 73, 587 (1993);
D. Prichard and J. Theiler, *Physica D* 84, 476 (1995)
- [19] P. Dutta and P.M. Hom, *Rev. Mod. Phys.* 53, 497 (1981)
- [20] B.J. West and W. Deering, *Phys. Rep.* 246, 1 (1994)
- [21] P. Bak, C. Tang, and K. Wiesenfeld, *Phys. Rev. Lett.* 59, 381 (1987);
P. Bak, *How Nature Works { the Science of Self-Organized Criticality*, (Copernicus, Springer-Verlag, New York, 1996)
- [22] P. A. Istrom and D. Stassinopoulos, *Phys. Rev. E* 51, 5027 (1995)
- [23] D. Stassinopoulos and P. Bak, *Phys. Rev. E* 51, 5033 (1995)

FIGURE CAPTIONS

Fig. 1. Sensor arrangement, signal and sensitivity profile of Virtual Sensor. (a) Coronal and sagittal views showing the sensor arrangement relative to the head and brain. (b) The average MEG signal for tone presentation to the left ear in the channels of the left and right probe. The channels with the strongest positive and negative signal are marked for each probe. The difference of weighted sums of channels, with weights decreasing with distance away from the highlighted channels define the Virtual Sensor. (c) By combining the sensitivity profile (lead field) of each channel according to how the channel is weighted in the VS sum, we obtain the sensitivity profile of the VS, which is clearly focussed in the auditory cortex.

Fig. 2. Three randomly selected raw MEG time-series (dashed, dash-dotted and dotted lines) versus the average over the whole set of 120 of them for the subject JD and left ear stimulation. Upper part illustrates the right hemisphere and lower part the left hemisphere behavior.

Fig. 3. Time-delayed MI as a function of the frequency (frequency window of 5 Hz) for subject JD, left ear stimulation.

Fig. 4. Two examples of the q -dependence of generalized MI (for $q = 1; 2; 4$ and 6). Upper part corresponds to JD (strong correlations) and lower part to FB (weak correlations).

Fig. 5a. $q = 6$ MI as a function of the time-delay for all ve subjects calculated from the time-interval between 0 (stimulus onset) and 250ms. Left column corresponds to the experiment Ex1a and right column to the experiment Ex1b. Solid line displays the response to the left ear, dashed line to the right ear and dash-dotted line to the binaural (only Ex1a) stimulation.

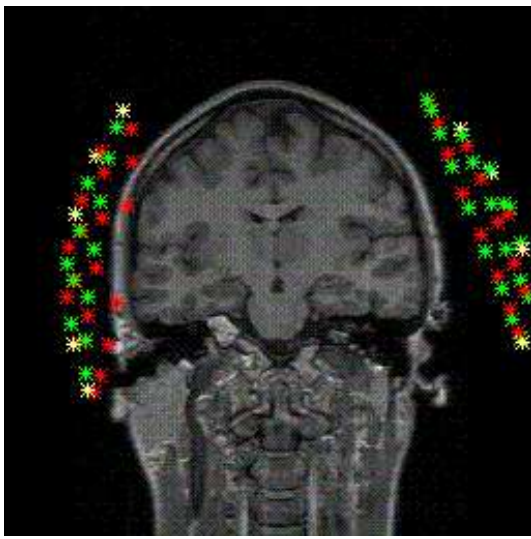
Fig. 5b. The same as Fig. 5a calculated from the 230ms long time-interval starting 230ms before the stimulus onset.

Fig. 5c. The same as Fig. 5c calculated from the time-interval between 251ms and 500ms.

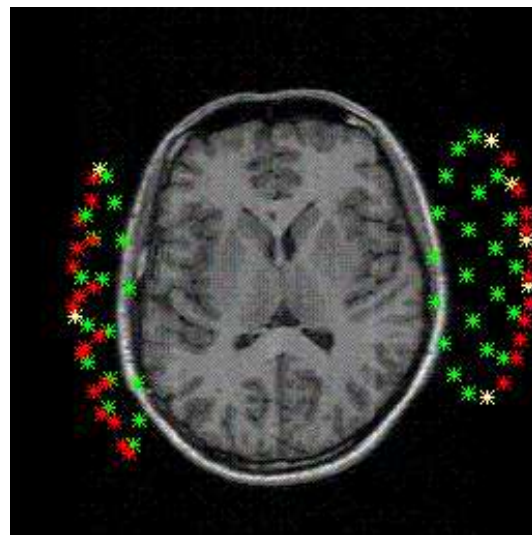
Fig. 6. The averaged MEG time-series over all 120 trials for four different subjects corresponding to the left ear (LE), right ear (RE) and binaural (B) stimulation. The solid line displays the left hemisphere and the dashed line the right hemisphere response.

Fig. 7. Power spectrum of the full MEG time-series. The upper part illustrates a typical behaviour for JD and the lower part for FB. The deep at 50 Hz is due to the notch filter applied at this frequency.

Fig. 8 Two examples (for JD and FB) of $q = 6$ MI between the time-series representing different trials, i.e., $x_L(t)$ is correlated with $x_R^+(t)$. The solid line corresponds to $\tau = 0$ (original case), $\tau = 1$ to the dotted line, $\tau = 4$ to the dash-dotted line and $\tau = 10$ to the dashed line.

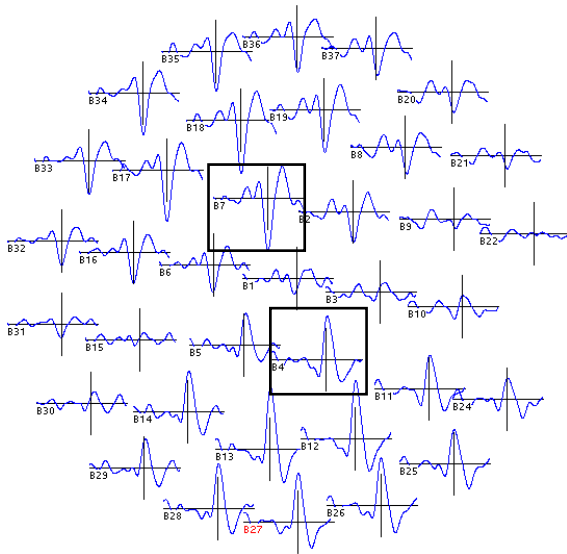


L R

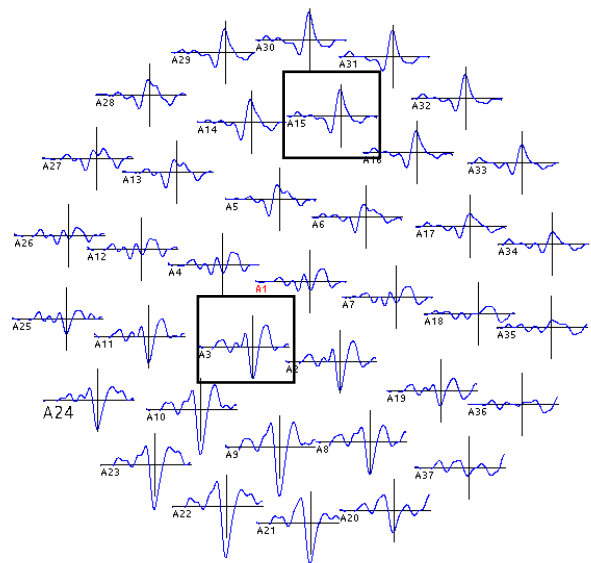


L R

(b) Average signals

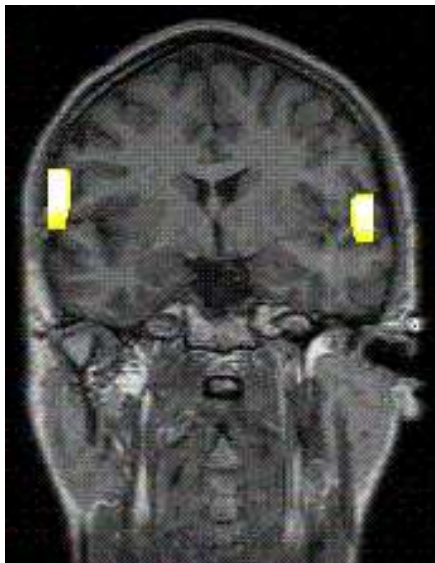


left hemisphere

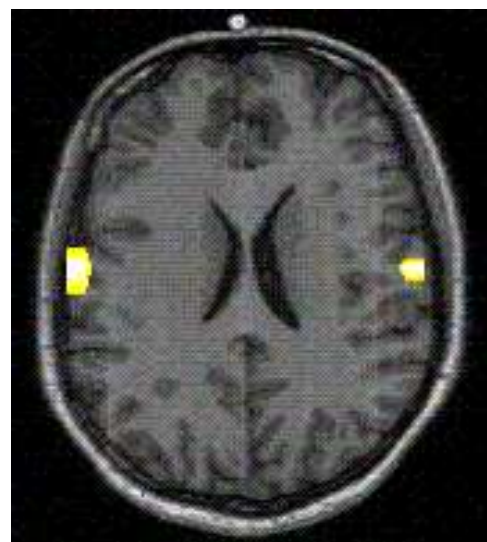


right hemisphere

(c) Sensitivity profiles of virtual sensors



L R



L R

